Electron impact dissociation of molecular hydrogen and deuterium: Production of atomic hydrogen and deuterium α, β, and γ Balmer lines*

George A. Khayrallah

Joint Institute for Laboratory Astrophysics, University of Colorado and National Bureau of Standards, Boulder, Colorado 80309

(Received 8 December 1975)

The absolute cross section for production of atomic Balmer α, β, and γ radiation by dissociative electron collisions with molecular hydrogen and molecular deuterium has been measured from threshold to 540 eV. Also measured are some absolute cross sections for the excitation of a few molecular lines. All of the cross sections for dissociation show some structure just above threshold. Below this structure, dissociative excitation is interpreted as proceeding through both predissociation and direct dissociation via a bound state above the dissociation limit of the molecule. Above this structure, dissociation proceeds through production of the unbound doubly excited $^1\Sigma_g^+$ and $^3\Sigma_u^+$ states of H_2. It is also argued that excitation of these doubly excited states is the major channel for production of excited atomic states in addition to being the major channel for production of protons by electron collisions with the molecule. Indeed its relative contribution increases with an increase of the principal quantum n. This contribution follows an inverse power law of 5.0 ± 0.5. Dissociation via the bound states depends on n with an inverse power law of 6.5 ± 1.0. The cross sections for production of excited deuterium atoms were found to be less than those for production of excited hydrogen atoms in the corresponding states, and the ratio varied from ~ 0.5 below 30 eV to ~ 0.82 at high energies, again indicative of three competing processes for dissociative excitation of the molecular target gas.

I. INTRODUCTION

In bimolecular dissociation by election impact on H_2 three distinct processes lead to an atomic product H(nl): (i) Pure dissociation,

$$e + H_2 \rightarrow e + H(n_1 l_1) + H(n_2 l_2);$$

(ii) dissociative ionization,

$$e + H_2 \rightarrow 2e + H(nl) + H^+;$$

and (iii) dissociative attachment,

$$e + H_2 \rightarrow H(nl) + H^-.$$

A number of measurements have been based on detection of charged products. Schulz and Asundi[1] measured the total cross section for process (iii) by detecting the negative ions. They found that the peak cross section is only 1.8×10^{-21} cm^2 for molecular hydrogen, while the cross section for molecular deuterium is nearly two orders of magnitude smaller. Many measurements of the cross section for dissociative ionization, i.e., process (ii), have been performed.[2] These measurements concentrated on the cross sections for production of protons, and did not look at the final states of the resultant atoms selectively.

Processes (i)–(iii) have been studied more selectively for production of excited atoms H(nl) and fall into three categories; the first and most extensively studied is dissociation of H_2 and D_2 to give a metastable atom in the 2s state.[3,4] The second is dissociation of H_2 into long-lived high-Rydberg fragment atoms.[5] The third, more general, set includes those dissociative processes leading to production of the Balmer-series fluorescence by atoms with principal quantum number 3, 4, 5, 6, etc. Williams *et al.*[6] and Burrows and Dunn[7] reported measuring the cross section for production of Balmer α, β, γ lines of hydrogen in the energy range 0–400 eV. Vroom and de Heer[8] measured the cross section for production of Balmer α, β, γ, and δ lines of hydrogen and deuterium in the energy range 50–6000 eV. They found some structure in the Balmer α lines of H and D which is different from that found in Ref. 5; they also noted that the cross section for dissociative production of excited H atoms was larger than that for production of excited D atoms at a given energy. Weaver and Hughes,[9] using time-resolved spectroscopy, tried measuring the relative contribution of the different obital states to the fluorescence of Balmer α and β radiation for energies between 20 and 400 eV. Their total cross sections were 25% lower than those of Vroom and de Heer[8]; furthermore, they did not see any structure in the cross sections at low energies. Julien *et al.*[10] and Glass-Maujean[11] used a level anticrossing technique to measure the relative ratios for dissociative production of the 3s, 3p, 3d state of atomic hydrogen. The relative ratios were in disagreement with the results of Weaver and Hughes.[9] Walker and St. John[12] mentioned measuring the total cross section for Balmer α, β, γ, δ, and ϵ emission at high pressures (20 mTorr); however, they gave no numerical results except at 200 eV. Richardson *et al.*[13] looked at the H_α line excited in electron collisions

with molecular deuterium; they found structure at 25 eV but discounted it as interference from molecular lines. Using microwave resonance spectroscopy they measured the relative $3s$, $3p$, $3d$ contribution to the H_α line. Their results disagree with the results of Refs. 9–11.

The results described in this paper arose as part of a project to extend the method of Mahan and co-workers [14–16] for resolving s-, p-, and d-state radiation from atomic hydrogen by direct electron excitation of the atom. In the present study the Balmer H_α (6563 Å), H_β (4861 Å), H_γ (4341 Å) emission cross sections for molecular hydrogen and molecular deuterium were measured in the course of ensuring proper operation of the apparatus, and considerable care was exercised. This study concentrated on the details of the excitation functions at low energies, the isotopic dependence of the process, and the subtraction of the molecular background. Preliminary results of the present work[17] and of similar measurements by Freund *et al.*[18] have been given.

A description of the apparatus is given in Sec. II, the experimental procedures as well as the cross sections for the excitation of molecular hydrogen are detailed in Sec. III, the determination of the absolute cross sections is presented in Sec. IV, and the data for H_2 and the discussion concerning the physical processes that lead to dissociation are given in Secs. V and VI, respectively. In Sec. VII the data for D_2 are compared with the H_2 data. In Sec. VIII a derivation is given for a possible dependence of the cross section for dissociation on some power of the principal quantum number of the dissociation product atoms.

II. APPARATUS

The present measurements of the Balmer emission cross sections were carried out in a crossed-beam apparatus described by Long *et al.*[19] and modified by Mahan *et al.*[14] for the detection of the Balmer line series.

The experiment, represented schematically in Fig. 1, consisted of scattering an electron beam from a molecular hydrogen or deuterium target, and the selective observation of the resultant fluorescent Balmer radiation through appropriate three-cycle interference filters whose optics axis was normal to the electron beam. Two target configurations were used: a static gas target, and a molecular beam target whose axis was perpendicular to the electron beam axis and to the optical axis of the detection system.

The electron beam was produced and formed by a Soa-type electron gun[20] with an indirectly heated type-A Phillips cathode. The electron energy

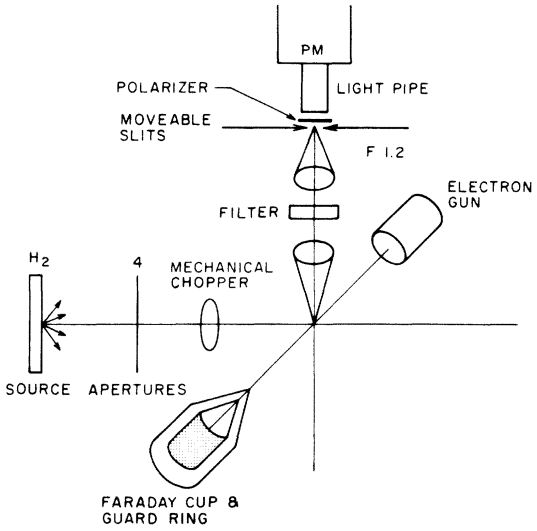

FIG. 1. Schematic diagram of the apparatus. The electron beam axis, the atomic beam axis, and the photomultiplier assembly axis are mutually orthogonal.

could be varied between 10 and 540 eV. The electron current was kept below 20 μA although currents up to 1 mA could be produced. The electron beam was cylindrical with a diameter that changed from 0.05 cm at 500 eV to 0.09 cm at 15 eV. The electron beam flux varied from 0.01 to 0.003 A/cm^2, leading to a space-charge voltage depression at the center of the beam with a magnitude of 0.6 V at 15 eV and 0.2 V at 500 eV. The full width at half-maximum of the electron beam energy distribution was measured to be 0.35 eV.

Hydrogen and deuterium of 99.9% purity (as specified by the manufacturer) were used as target gases. In the case of a molecular beam target, the gas was fed through a palladium leak. In the collision region the thermal beam had a square cross section with an umbra 0.5 cm to a side and a penumbra 0.65 cm to a side. The molecular beam density in the umbra region was approximately 3×10^8 molecules/cm^3, while the residual background gas density was also 3×10^8 molecules/cm^3 (corresponding to a pressure of 10^{-8} Torr), thus necessitating modulation of the molecular beam target and the detection of the resultant modulated component of the resultant signal. A chopper located between the molecular beam effusion source and the collision region caused complete modulation of the beam at 100 Hz with a 50% duty cycle. When a static target gas was used, the gas was continuously fed into the interaction region through a leak valve and the chamber was continuously pumped by a liquid-nitrogen baffled 6-in. mercury diffusion pump. The pressure in the interaction region, typically

corresponding to 1×10^{11} molecules/cm^3, was monitored by a triode ionization gauge[21] at pressures below 1×10^{-4} Torr, and by a nude Varian Millitorr gauge[22] at pressures larger than 5×10^{-6} Torr. The Millitorr gauge was calibrated[23] against a McLeod gauge, and it was used to calibrate the triode ionization gauge at the lower pressures.

The interaction region was shielded by two layers of Conetics magnetic shielding, thus reducing the magnetic field to less than 10 mG. The region was also coated with Aquadag, which provides a relatively uniform potential surface as well as decreasing the reflection of light inside the interaction region.

Radiation from the interaction region was detected by a dry-ice-cooled photomultiplier[24] through an optical assembly with $f/1.2$ optics. The photomultiplier had a gallium-arsenide photocathode with an enhanced S-128 response.[24] The optical system[14] was modified to allow the insertion of a rotatable HN-38 polaroid polarizer perpendicular to the optical axis. A refined slit mechanism, accurate to 2.5×10^{-3} cm, was also included in the image plane to allow a scan of either the shape of the fluorescent light from the interaction region or the light from a silver target held in the path of the electron beam. This mechanism was used to determine the extent and shape of the electron beam as well as the extent of the interaction volume. The different Balmer α, β, and γ emission lines were selected by appropriate three-cycle interference filters whose bandwidths at half-maximum were 15, 11, and 18 Å, respectively, and whose peak transmissions were centered at the emission lines. Provisions were made to tilt these filters for non-normal entry, thus allowing fine tuning of the central wavelengths of the filter by approximately -10 Å. Other filters were also used to measure the molecular background light.

The output pulses from the detector could be counted with an 80-MHz fast-counting system; alternatively, the time-averaged current output of the photomultiplier could be measured with standard electrometers and lock-in amplifiers. A small incandescent lamp was also included in the vacuum system facing the photomultiplier in order to monitor the gain of the detection system as a function of time.

III. EXPERIMENTAL PROCEDURE

In measuring excitation functions and their corresponding emission cross sections one has to be sure that all the spurious backgrounds are subtracted, that the energy scale does not vary with current and pressure, that the signal is linear with both pressure and electron beam current simultaneously, that all stray electric and magnetic fields are negligible (especially for states with large quantum numbers), and that the fraction of the light collected from the interaction region is constant for all energies. The remainder of this section describes these corrections and tests.

A. Linearity with electron current

The electron beam current was varied between 1×10^{-7} and 2×10^{-4} A. Since mixing and quenching of H(nl) states depend linearly on the square of the electric field, and since the electric field produced by a cylindrical electron beam depends linearly on the electron beam current carried by the cylinder, the signal divided by the electron beam current (a quantity proportional to the measured cross section) was plotted against the square of the electron current. In the present electron current range the measured cross section decreased linearly as the square of the electron current was increased, with a slope that did not exceed 1×10^{-24} cm$^2/\mu$A^2. At all energies, a small current of less than 20 μA was used. This leads to less than 1% correction to the measured cross sections.

B. Linearity with target pressure

When a molecular beam target was used, nonlinearities with beam density ($\sim 3\times10^8$ molecules/cm^3) were not observed. However, as the static target gas pressure was increased through the range of densities from 3×10^8 to 3×10^{15} molecules/cm^3, both the cross sections and the threshold energies changed. The changes were caused

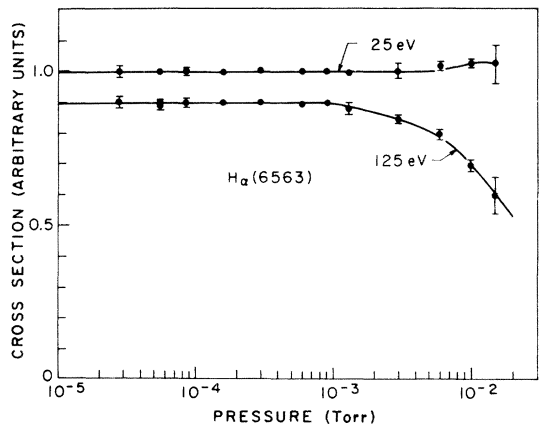

FIG. 2. Plot of the measured relative Balmer-α emission cross section as a function of the absolute pressure of the molecular hydrogen target. The top curve was measured at 25 eV incident electron energy; the lower curve was measured at 125 eV incident electron energy.

by (1) multiple collisions of the electrons, thus destroying their monochromaticity, (2) the change in the work function of the electron gun cathode due to poisoning and cooling by the target gas, and (3) the production of ions in the target gas. The cross section for Balmer α emission versus pressure is shown in Fig. 2. Nonlinearities start setting in at approximately 10^{-3} Torr. Similar dependence has been observed and predicted by Wilcox and Lamb.[25] Independently, Heddle[26] predicted that at 10^{-3} Torr ion production will be sufficiently large to cause secondary processes in the collision region, as well as to cause an actual shift and spreading of the observed threshold energy for production of emission lines. In the measurement presented here pressures were kept at 5×10^{-6} Torr or less, to ensure linear dependence of the cross section on the pressure.

C. Effects of electric and magnetic fields

The effects of electric and magnetic fields have been discussed by Lamb and Sanders[27] and by Wilcox and Lamb.[25] They showed that the presence of electric or magnetic fields changes the amount of light collected in the detection system. The main cause was the mixing of the different fine-structure states of the excited atom, thus leading to a change in the branching ratios for emission. Wilcox and Lamb[25] have found that the presence of a magnetic field of less than 50 G increased the amount of H_α line observed. Magnetic shielding was used in the present work to limit fields to 10 mG or less.

A method similar to that of Mahan *et al.*[14] was used to test for electric field effects. Fields were applied in the interaction region along the three axes of the machine. It was found that the application of any electric field bigger than 0.02 V/cm in any direction changed the cross section symmetrically about the no-applied-field case (at 0.02 V/cm the range in H_α was about 5%). This established that coating with Aquadag, and careful shielding of the power leads, successfully created a free-field interaction region.

D. Variation of light collection efficiency

Since atoms are produced in different orbital states, each with a different lifetime, photon collection efficiency for states with long lifetimes may be somewhat lower than for short-lived states. Since no theoretical estimates exist for the cross section being measured, accurate calculation of the collection efficiencies cannot be carried out. The Appendix presents estimates for collection losses of each individual *nl* state.

However, the interaction region could be scanned in a direction perpendicular to the electron beam axis to search for radiation displaced from the excitation volume (electron beam).
The scan was performed with a rectangular slit formed between two independently adjustable knife edges that moved in a direction orthogonal to the electron beam axis. By observing radiation excited by the electron beam impacting a silver target inclined at 45° to both the optics axis and the electron beam axis, and by observing the resultant radiation, a determination of the electron beam shape and relative axial density could be obtained.[15,17] Observations of the distribution of radiation with gas in the system allow one to estimate the number of radiating atoms that drifted from the field of view of the optical system, approximately 0.254 cm wide. Figure 3 shows a plot of the measured intensity distribution. In most cases less that 3% of the excited atoms decayed beyond the region of observation and detection.

E. Energy scale

The energy scale was fixed by the measurements of the known threshold of 23.067 eV for the excitation of the $3\,^1D \rightarrow 2\,^1P$ (6678-Å) line in helium. The method involved using a transmission filter[28] centered at 6678 Å and with a bandwidth of 100 Å full width at half-maximum (FWHM). Hence a mixture of 70% H_2 (at the operating pressure) and 30% He was used. The concentration of helium did not affect the position of H_2 threshold significantly (to within 0.1 eV).

The results of this calibration agreed with the calculated thresholds for the dissociation of H_2

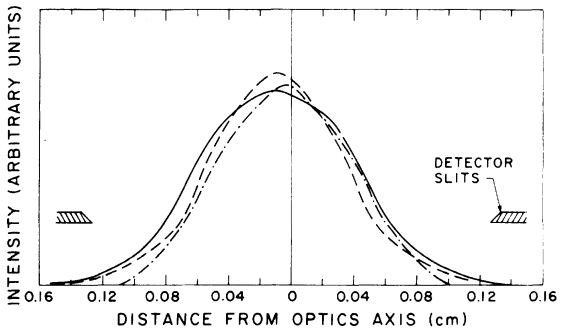

FIG. 3. Plot of the measured relative emission density of photons caused by electron impact. The resolution is 0.0025 cm. The dash-dot line shows the detection of 4070-Å radiation caused by scattering of the 500-eV electron beam by a silver target. The remaining two curves are for H_α radiation caused by 80-eV (– – –) and 50-eV (——) electron excitation of molecular hydrogen.

and D_2 to within 0.2 eV. The calculated thresholds for dissociation were taken to be

$$H_2 \rightarrow H(1s) + H(3s),\ 16.56\ \text{eV} \quad (1)$$

$$\rightarrow H(1s) + H(4s),\ 17.22\ \text{eV} \quad (2)$$

$$\rightarrow H(1s) + H(5s),\ 17.53\ \text{eV}. \quad (3)$$

F. Molecular radiation subtraction

Molecular radiation caused by electron impact is a source of background radiation that may interfere with the observed atomic lines. Many studies[29,30] have been made on the molecular continuum and line radiation in the visible region, but all of these studies were performed in high-pressure H_2 discharges. Thus their results are not useful for background subtraction in the present study. It was found that the most intense molecular radiation occurred at energies below 30 eV,[29,30] the most intense lines occurred at around 6000 Å,[29,31,32] and the continuum radiation intensity peaked at around 2600 Å,[30] with an almost inverse dependence on the wavelength at higher wavelengths.[30]

i. H_α *(6563 Å).* At this wavelength, and within the 15-Å FWHM pass band of the interference filter used, no strong molecular lines are present[31,32]; however, the many-line radiation spectrum contributed to the background. To measure this contribution two filters were used, one a sodium-line filter (central wavelength 6710 Å, FWHM 10 Å), the other a helium-line filter (central wavelength 6678, FWHM 100 Å). It was found that the two filters gave the same result for the molecular radiation intensity per unit wavelength interval. Assuming that the same density holds at 6563 Å, then less than 1.6% background radiation contributed to the measured H_α (6563 Å) signal. A plot of the molecular emission excitation cross section per unit wavelength is shown in Fig. 4.

ii. H_β *(4861 Å).* Within the 11-Å FWHM bandwidth of the filter used, only one molecular line (the 4856.55-Å line) is of sufficient intensity to contribute background. The 4856-Å line radiation appeared at the bottom of the threshold region for H_β excitation, with a magnitude of approximately 4%. Hence a study of the line radiation versus energy was conducted using another filter[28] (central wavelength 5047 Å, FWHM 100 Å). Contributions from ten strong molecular lines[31,32] as well as the continuous molecular background were observed through this filter at the same time. Thus the radiant density per unit wavelength of molecular light received by this filter was close to that received by the H_β filter. A plot of the electronic molecular emission excitation cross section per unit wavelength is shown in Fig. 4 for H_2 targets. The contribution to the measured H_β excitation cross section was less than 2% above 30 eV and approximately 12% at 20 eV.

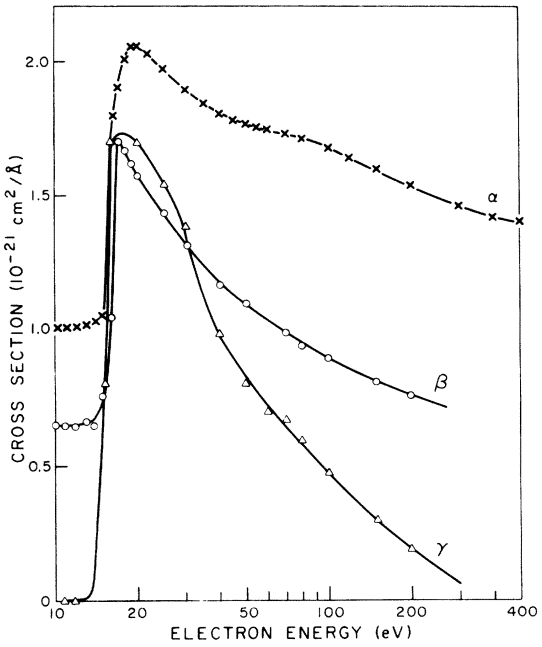

FIG. 4. Measured absolute emission cross section density per molecule per angstrom for molecular light emission as a function of incident electron energy. The —×— curve refers to light detected through an interference filter with 100-Å FWHM centered at 6678 Å. The open circles refer to light detected at 5047 Å with a 100-Å FWHM bandwidth interference filter; —△— refers to light observed through a 50-Å FWHM interference filter centered around 4070 Å. α, β, and γ refer to the atomic Balmer lines from which that molecular curve was subtracted.

iii. H_γ *(4340.5 Å).* No strong molecular lines exist in this wavelength region (the closest are 110 Å on each side), but the molecular continuous background is large. Since a filter close to 4340 Å was not readily available, the filter centered at 4070 Å (50-Å FWHM, used to observe the fluorescence from the silver target) was utilized. The observed excitation cross section per unit wavelength within that band is plotted in Fig. 4. The molecular contribution to the H_γ lines as observed by the H_γ filter with an 18-Å FWHM was approximately 65% at 18 eV, 10% at 70 eV, and 1% at 120 eV. Since the measured background was far from the H_γ line, only the measured energy dependence of the molecular radiation at 4070 Å was used to correct for the continuum contribution to the H_γ excitation curve. See Sec. V C.

G. Polarization effects

To extract a cross section from a measurement, the polarization, and hence the angular distribution, of detected light must be measured. An initial measurement using an HN-38 polaroid polarizer showed that at threshold the polarization of the light relative to the electron beam axis was 0.00 ± 0.05. As the energy increased to 50 eV the polarization of the light became 0.10 ± 0.05 and at 500 eV the polarization changed sign to -0.05 ± 0.02. Though the measurement of the polarizations was rough, it agreed with the observation of Vroom and de Heer.[8] Because of the small degree of polarization no correction for polarization was included in the cross sections.

IV. ABSOLUTE CROSS-SECTION DETERMINATION

The measurements of the absolute cross sections were made using a static target gas. This required the calibration of the pressure measuring instruments and of the optical detection assembly. The pressure measurement instrument was calibrated[23] versus a McLeod gauge. The ionization cross section and ion gauge collection efficiency for H_2 and D_2 gases were taken to be the same. The main sources of error are ascribed to uncertainties in the exact temperature of the gas, and the errors due to hysteresis in the ion gauges. The pressure measurement is the source of the largest uncertainty, and it is estimated to be accurate to within 10%.

The optical detection system was calibrated in the manner described by Taylor,[33] using some of his instrumentation. Briefly, a secondary portable source of monochromatic radiation consisting of a stable incandescent light source, monochromator, and a diffusing and depolarizing sphere was calibrated versus a blackbody standard. The spectral radiance of this sphere was measured by Taylor[33] at 6563, 4930, 4800, 4550, 4350, 4050, and 3931 Å to within 5% accuracy. Linear interpolation was used to calculate the spectral radiance in photons $\sec^{-1}\,\mathrm{sr}^{-1}\,\text{Å}^{-1}\,\mathrm{cm}^{-2}$. When this source was put in the focus of the detection assembly (the normal position of the scattering region), the count rate measured was given by

$$C_R(\lambda_M) = \eta \int\int\int\int L(\lambda) t(\lambda,\lambda_M) S_D(\lambda)\, dx\, dy\, d\Omega\, d\lambda, \tag{4}$$

where λ_M is the wavelength of interest, η is the electronics efficiency (dependent on, e.g., the position of the pulse-height discrimination level), $L(\lambda)$ is the spectral radiance of the reference, and $t(\lambda,\lambda_M)$ is the transmission function of the monochromator. $S_D(\lambda)$ is the efficiency of the detection assembly given by

$$S_D(\lambda) = \Omega(x,z)\epsilon(\lambda,x,z)\, T(\lambda), \tag{5}$$

where Ω is the solid angle subtended by the source from a point x,z inside the observed area, $\epsilon(\lambda,x,z)$ is the photomultiplier detection efficiency for given wavelength λ at position x,z, and $T(\lambda)$ is the transmission of the filter used. If one assumes that $L(\lambda)$, $T(\lambda)$, $\Omega(x,y)$, and $\epsilon(\lambda,x,z)$ vary little with λ near the peak of the reference emission at λ_M and with x,z across the emitting surface, then

$$C_R(\lambda_M) = \eta\epsilon(\lambda_M) T(\lambda_M) L(\lambda_M) A I_s \Omega, \tag{6}$$

where A is the area of a hole in the diffusing depolarizing sphere from which light is detected,

$$I_s = \int_{-\lambda_0}^{\lambda_0} t(\lambda,\lambda_M)\, d\lambda$$

is the area under the transmission function of the monochromator, and λ_0 is the cutoff wavelength of the monochromator slit function. Using the measured $t(\lambda,\lambda_M)$ and λ_0, Taylor[33] calculated the values $I_s = 2.47\ \text{Å} \pm 2.5\%$ for $\lambda_0 = 50\ \text{Å}$.

If one now looks at the signal seen when the electron beam hits the target gas, the count rate is given by

$$C_S(\lambda_M) = \eta \int\int\int\int dx\, dy\, dz\, T(\lambda_M) \frac{d\Omega(x,y,z)}{4\pi} \times \epsilon(\lambda_M,x,y)\sigma F(x,y,z)\rho(x,y,z), \tag{7}$$

where σ is the required cross section, ρ is the density of the gas, and F is the electron flux density (the number of electrons per second crossing a unit area perpendicular to the electron beam direction). Again if one assumes that Ω varies little over the detection volume, that the density of the gas is uniform, and that the photomultiplier efficiency varies little with x, y, z, then

$$C_S(\lambda_M) = \eta\sigma\epsilon(\lambda_M)\frac{\Omega}{4\pi}\rho\, T(\lambda_M) \int\int\int dx\, dy\, dz\, F(x,y,z). \tag{8}$$

Since the electron density is independent of the position z along the electron beam,

$$C_S(\lambda_M) = \eta\epsilon(\lambda_M) T(\lambda_M)\Omega\sigma l\rho n/4\pi, \tag{9}$$

where l is the length of the electron beam seen by the photomultiplier and n is the number of electrons per second crossing the interaction region. Thus

$$\frac{C_S(\lambda_M)}{C_R(\lambda_M)} = \frac{\sigma(\mathrm{cm}^2)\rho(\text{molecule/cm}^3) l(\mathrm{cm}) n(\text{electron/sec})}{4\pi A(\mathrm{cm}^2) I_s(\text{Å}) L(\text{photon/sec cm}^2\,\text{Å})}, \tag{10}$$

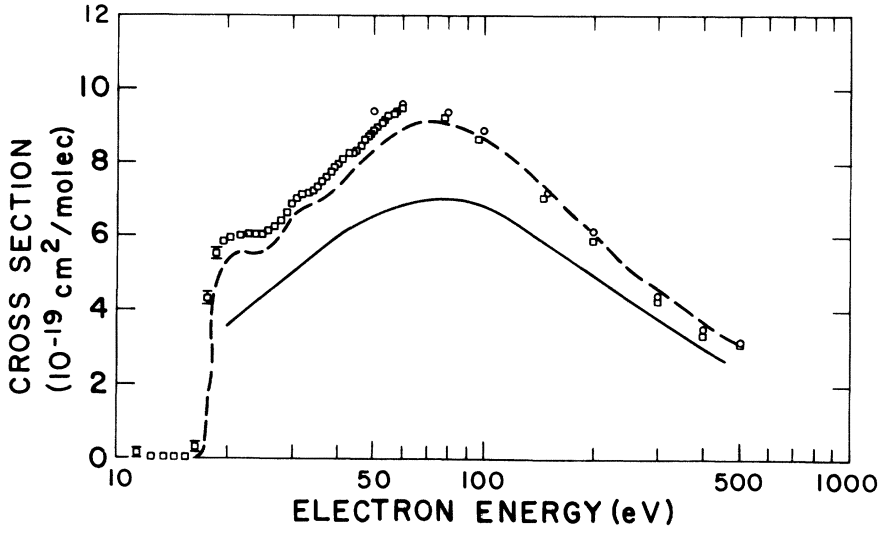

FIG. 5. Absolute cross section measured for H_α emission during e-H_2 collisions. □: present measurement; ○: Vroom and de Heer (Ref. 8); ---: Williams *et al.* (Ref. 6); —: Weaver and Hughes (Ref. 9). The data of Williams *et al.* (Ref. 6) were normalized to those of Vroom and de Heer. (Ref. 8) at 500 eV.

a result independent of the detection efficiency, solid angle, and filter transmission. This equation can be inverted to calculate the cross section in terms of measurable quantities. The major errors come from the measurement of ρ and $L(\lambda_M)$. The error in C_S and C_R did not exceed statistical errors, which could be reduced by repeated measurements to values less than 0.5%. The error in determining the current was less than 0.3%, stemming mainly from amplifier noise and secondary electron emission. The error in $L(\lambda_M)$ was 5.0%, while the error in determining l was 2%, mainly owing to the large aperture of the lens. The error in determining A was less than 0.5%, mainly owing to the accuracy with which we can move the imaging slits and position the diffusing and depolarizing sphere. If a 10% error in ρ, as well as the 2.5% error in I_s, and a 2% error for atoms escaping the detection region are included, then the quadrature of these errors leads to 11.8% error. The cumulative sum of all errors is 23%, where the polarization and cascade corrections have not been included in either error analysis.

V. MEASURED DATA

The results of the measurements of the cross sections for H_α, H_β, and H_γ radiation are shown in Figs. 5 – 7, respectively. The uncertainty in the present results for each cross section amounts to 12%. The figures also show the absolute cross sections measured by Vroom and de Heer[8] and Weaver and Hughes,[9] as well as the results of Williams *et al.*[6] normalized[34] to those of Vroom and de Heer.[8] All of the cross sections plotted in Figs. 5 – 7 are not corrected for either

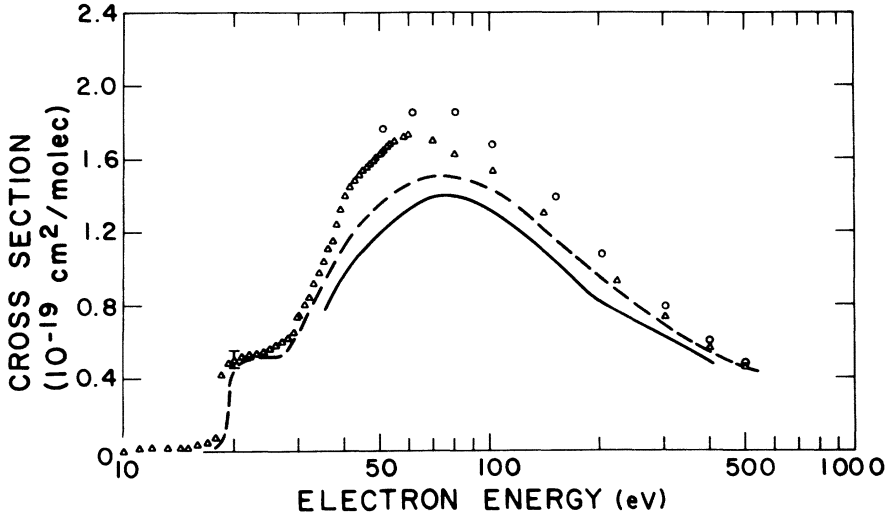

FIG. 6. Absolute cross section for H_β emission during e-H_2 collisions. △: present data; ○: Vroom and de Heer (Ref. 8); —: Weaver and Hughes (Ref. 9); ---: Williams *et al.* (Ref. 6). The data of Williams *et al.* (Ref. 6) were normalized to the data of Vroom and de Heer (Ref. 8) at 500 eV.

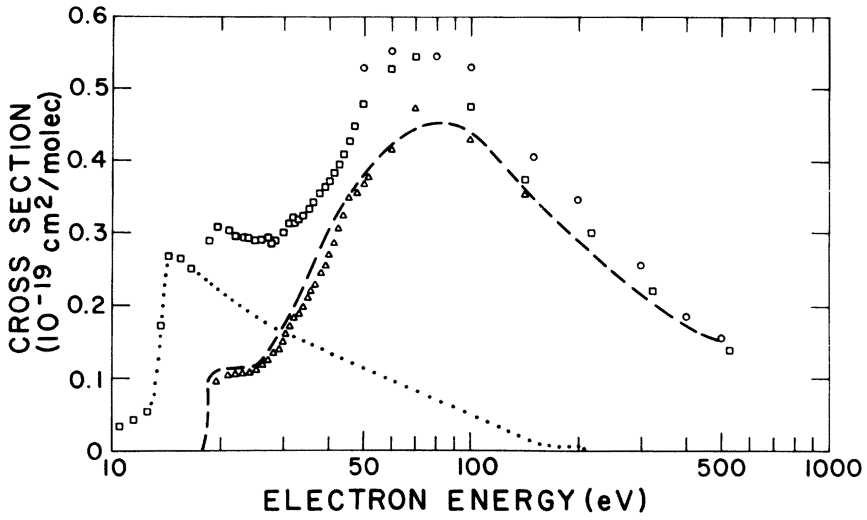

FIG. 7. Absolute cross section for H_γ emission during e-H_2 collisions. ○: Vroom and de Heer (Ref. 8); ---: Williams *et al.* (Ref. 6) normalized at 500 eV to the data of Vroom and de Heer (Ref. 8); □: present measurement with no molecular background correction; • • •: measured molecular emission cross section scaled to remove its contribution below the H_γ threshold exactly; △: present measurement corrected for molecular background.

polarization or cascades. The present cross sections were measured at 1-eV intervals for energies below 60 eV, as well as at a few energies between 80 and 540 eV.

A. H_α (6563 Å)

The present data (12% uncertainty) seem to agree very well in shape as well as in magnitude with the results of Vroom and de Heer[8] (estimated uncertainty 12%) over the common energy range. The data of Weaver and Hughes[9] (estimated uncertainty 25%) lie below the present data at all energies, and do not show the structures observed in this experiment at energies below 40 eV. The normalized data of Williams *et al.*[6] agree with the present data at energies above 80 eV, and although below 80 eV their data are slightly lower (by an almost constant value of 0.4×10^{-19} cm^2), there is still excellent agreement between the shape of the cross sections. The single datum point of Walker and St. John[12] at 200 eV lies between the present data and those of Vroom and de Heer.[8] The threshold for the present cross section was found to lie at 16.60 ± 0.1 eV, in agreement with the theoretical value of 16.56 eV for dissociation into two atoms with zero kinetic energy. The peak of the cross section occurred at about 70 eV.

B. H_β (4861 Å)

The present results[35] show agreement with the results of Vroom and de Heer[8] at 400 and 500 eV. However, below 300 eV the present results are lower than those of Vroom and de Heer,[8] but the difference is still within the combined experimental errors of the two measurements. Again the present results are larger than those of Weaver and Hughes.[9] The results of Williams *et al.*[6] agree with the present results throughout the energy range except between 40 and 70 eV, where the present cross section is larger than theirs by about 20%. The datum of Walker and St. John[12] at 200 eV is 20% larger than the present result; however, they give no estimate of the uncertainty in their measurement.

The threshold for the H_β production cross section was measured to be 17.25 ± 0.1 eV, in agreement with the theoretical value of 17.22 eV. The peak of this cross section occurred at about 65 eV.

C. H_γ (4341 Å)

Figure 7 shows the present data for H_γ production. The open squares are the present data uncorrected for the molecular background. The dotted line shows the measured molecular background scaled to eliminate its contribution below 17.53 eV, the threshold for dissociation. The open triangles show the resultant cross section after the subtraction of the background molecular light. It is seen that the contribution of the molecular light is significant and should be subtracted from any measurement at these short wavelengths. One notes that the molecular background radiation has a threshold of approximately 12.7 $\pm$ 0.3 eV, the threshold for exciting the $C^1\Pi_u$ ground vibrational state of H_2.[36]

The data of Vroom and de Heer[8] (7% estimated uncertainty) are seen to be higher than the present data at all energies. Serious differences exist at the lower energies. The difference cannot be explained except by the probable existence of molecular radiation in their data, or by the inadequacy of their electron gun at low energies. Similar differences have been noted by Cox and

Smith[4] for the Ly-α cross sections. The absolute datum point of Walker and St. John[12] at 200 eV was 25% larger than the present measurement. The normalized data of Williams *et al.*[6] seem to agree very well, both in shape and in magnitude, with the present data, especially at the low energies.

It is seen that the threshold for the H_γ emission occurs at 17.9 ± 0.2 eV, slightly above the theoretical value of 17.53 eV. The peak of the cross section occurs at 70 eV, very close to the peak in the H_α and H_β cross sections.

VI. H_2: DISCUSSION

One of the outstanding features of the measured cross sections is the shape of the excitation functions. It is seen that two thresholds exist in all the cross sections, the first occurring between 17 and 18 eV, and the other between 25 and 30 eV. This is indicative of at least two different processes that lead to excited hydrogen atoms. In the case of H_α production, a third threshold seems to exist at around 35 eV. Another outstanding feature of these cross sections is the variation of the ratio of magnitudes at their peak to their value at the plateau just above threshold with the principal quantum n.

Figure 8 is a schematic diagram of certain energy levels of H_2 and H_2^+ as a function of internuclear distance, where the origin of the energy is taken at the energy of the lowest vibrational state of $H_2(X^1\Sigma_g^+; v=0)$. The curves labeled $^3\Pi_g$, $^3\Sigma_u^+$, and $^1\Sigma_g^+$, and drawn with dashes, are some of the double excited repulsive states that may be involved in the present processes. The energies calculated for the $^3\Pi_g$, $^3\Sigma_u^+$, and $^1\Sigma_g^+$ states by Bottcher and Docken,[37,38] in agreement with the calculations of Hazi,[39] were added to the standard energy levels of H_2 as tabulated by Sharp.[40] Energies for other doubly excited states, such as the lowest $^1\Pi_u$ state, were not included, since at the present time there is disagreement between the different calculations[38,39] as to their energies and their assignments.

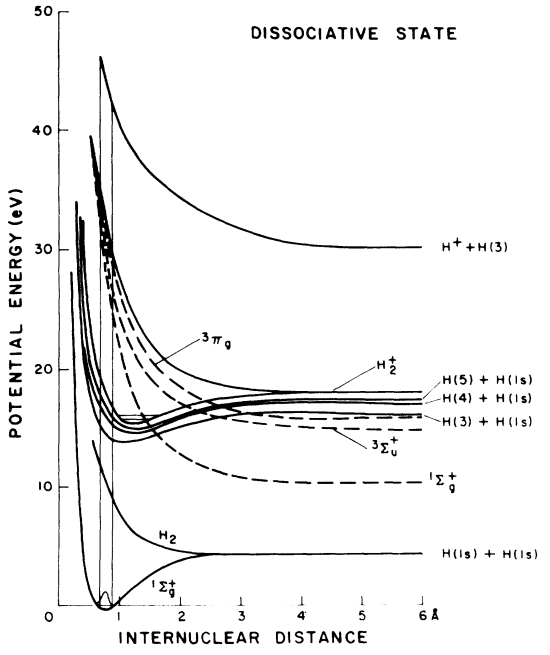

FIG. 8. Energy levels of molecular hydrogen as a function of the internuclear separation, omitting levels not relevant to discussions in Sec. VI of the text.

The levels diagrammed in Fig. 8 provide a basis for interpreting the observed structure by application of the Franck-Condon principle and by consideration of curve crossings. As the electron energy is increased it reaches a value such that excitations to the $(1s\sigma_g)(nl)$, usually bound molecular states are possible. These states correlate to H(1s) + H(nl) at infinite internuclear separations. Dissociation of these states into two hydrogen atoms with zero kinetic energy occurs when the energy supplied by the electron during the collision just exceeds[40] $18.076 - 13.598/n^2$ eV.

As the molecule separates, the energy levels of the $(1s\sigma_g)(nl)$ states cross the energy levels of either of two types of states, the diabatic repulsive doubly excited states of H_2, $^1\Sigma_g^+$, $^3\Sigma_u^+$, and $^3\Pi_g$ and the adiabatic $(2p\sigma_u)(n'l)$ repulsive states with $n'<n$, the crossing being dependent on the picture one is using to describe the dissociation of the excited H_2 molecule. These crossings lead to loss mechanisms, mainly to $H^- + H^+$ and H(1s) + H($n'l$) products, where $n' < n$. Both of these processes are predissociative processes.

A special case occurs when nl is a continuum state. Then, the H_2 molecule dissociates into $H_2^+(1s\sigma_g)$, the ground-state molecular ion, and a free electron. However, this ionizing state crosses the $^1\Sigma_g^+$ state and a transition can occur corresponding to the recapture of the electron by the proton into any of the atomic Rydberg states whose energy levels converge with or cross the $^1\Sigma_g^+$ energy level. This is a mechanism similar to a mechanism proposed by Schiavone *et al.*[41] for production of high-Rydberg atoms from autoionizing states of H_2.

As the energy of the electron is increased further, excitation of the lowest autoionizing doubly excited diabatic repulsive states of H_2 occurs[38] with a threshold of 24.5 eV for the $^1\Sigma_g^+(2p\sigma_u)^2$ state, 26 eV for the $^3\Sigma_u^+(2p\sigma_u)(2s\sigma_g)$ state, and 29 eV for the excitation to the $^3\Pi_g(2p\sigma_u)(3d\pi_g)$ state. The second threshold seen in the present measured

cross sections presumably arises in this way. The existence of these structures in the dissociative collision excitation functions was first predicted by Lamb and Rutherford.[42] They explained the existence of these structures in terms of dissociative doubly excited states of H_2. Later, Lamb and Sanders[27] and Wilcox and Lamb[25] observed the structure for dissociation into $n=3$ hydrogen atoms. By virtue of the discussion in Sec. V, these doubly excited repulsive states cross every $(1s\sigma_g)(nl)$ energy level with $n \geq 3$, while they all lie below the adiabatic $(2p\sigma_u)(nl)$ energies.[37, 38, 43] However, according to Dunn's[44] analysis of transitions between states of homonuclear molecules, no transitions can occur from the ground $^1\Sigma_g^+$ state to the excited $^3\Pi_g$ state. Of the remaining two states it seems likely that excitation to the $^1\Sigma_g^+$ is more probable than excitation to the $^3\Sigma_u^+$ state. As pointed out by O'Malley[45] and Bottcher[46] these diabatic states always furnish a mechanism for dissociation through highly probable transitions that occur at the crossing points of the diabatic potential curves with the normal Rydberg states of H_2. Even though dipole excitation of the $^1\Sigma_g^+(2p\sigma_u)^2$ state from the $X^1\Sigma_g^+$, $v=0$ state is forbidden, Bottcher and Docken[37] found that quadrupole transitions cause its excitation. Using a simple classical model, Hazi[47] calculated that 40% of the molecules excited to the $^1\Sigma_g^+(2p\sigma_u)^2$ state decay to the dissociation continuum, while 14% decay to the $H^- + H^+$ ion pairs. It was also found that the $^1\Sigma_g^+$ level is almost entirely responsible for dissociative recombination[48] of H_2^+ with electrons, as well as probably responsible for dissociative ionization of H_2 by electrons.[49, 50] Schiavone *et al.*[41] also argued that excitation to this state is one of the major mechanisms for producing high-Rydberg atoms in e-H_2 dissociative excitation.

As the electron energy is increased further, excitation to the repulsive adiabatic $(2p\sigma_u)(nl)$ states is possible above 31 eV. These states dissociate into $H(1s) + H(nl)$ and $H^-(ls,nl) + H^+$ in the limit of infinite internuclear distances. Yet these states autoionize to the $1s\sigma_g$ state of H_2^+, whose energy levels they cross at internuclear distances greater than 2.5 Å. It is not expected that these states will contribute very much to dissociation unless, within the Franck-Condon region, their autoionizing lifetimes are much larger than the dissociation time. Presently, not much is known about these lifetimes.

Finally, at still higher electron energies other channels contribute. Dissociation into two excited atoms sets in above 32 eV.[3] Dissociation into a proton plus an excited hydrogen atom sets in at approximately 41.5 eV,[40] the energy required to reach the $\pi_u 3s$ separated-atom state. The largest energy where the threshold exists is 47 eV, equal to the dissociation energy between two protons at 0.90 Å.

Of the previously mentioned processes, predissociation and direct dissociation predominate at low energies, predissociation being relatively more important for dissociation into lower states, since more vibrational states lying above the dissociation continuum contribute to the predissociating process. The products of the dissociation have a maximum energy of 0.4 eV [the difference between the maximum energy of the $(1s\sigma_g)(nl)$ state inside the Franck-Condon region at 0.6 Å and the final internal energy of the products at infinite internuclear separations]. This corresponds to a velocity of 8 km/sec, assuming that the energy is shared equally among the dissociation products. Similar velocities for the product particles have been observed experimentally by Glass-Maujean.[11] Predictions by Ford and Docken[51] for the velocities of ions formed through ionization to the $H_2^+(1s\sigma_g)$ state also indicate average proton energies of 0.22 eV. The $1s\sigma_g$ state is the limit of the $(1s\sigma_g)(nl)$ states of H_2, and is expected to have similar energy curves.

At the higher energies, it is seen that excitation of the $H_2(^1\Sigma_g^+(2p\sigma_u)^2)$ state with a threshold of 25–27 eV followed by dissociation is responsible for both Balmer emissions and high-Rydberg-state production. Since the dissociation energies lie between 16.5 and 17.5 eV, each final product carries approximately 4 eV of energy, corresponding to velocities of 35–40 km/sec. Again Glass-Maujean,[11] Lamb and Sanders,[27] and most recently Freund *et al.*[18] observed the effect of these atoms through their effect on the Doppler shift of absorbed and emitted radiation.

VII. D_2: RESULTS

The absolute cross sections for H_α, H_β, and H_γ emission cross sections during e-D_2 collisions have been measured for energies less than 100 eV. Previously, Vroom and de Heer[8] measured this cross section at high energies. They found that for Ly-$\alpha(2p)$, Ly-$\alpha(2s)$, H_α, H_β, and H_γ radiation the cross section for light emission from the dissociation of D_2 was smaller than that for H_2 by 20% for energies between 50 and 6000 eV. Similar isotope dependence was seen by Vroom and de Heer[52] in the production of Lyman and Balmer radiation in e-CH_4 and e-CD_4 dissociation. Burrows and Dunn[7] also reported a measurement, but no results were published; however, their data agree with the present results.

The experiment was performed at low energies.

The results are shown in Fig. 9, where the ratio of the cross sections for Balmer emission from H_2 to that for Balmer emission from D_2 are plotted. For H_α emission the ratio varies from 1.08 at threshold to 1.06 above threshold. The ratio does not tend to the value of 1.2 that Vroom and de Heer[8] had found, but the difference in these limits is well within the uncertainties of the two experiments. In the present measurement the estimated uncertainty is 11% in each cross-section measurement, and 14% for the ratio. It is interesting to note that the deuterium data showed structure near the thresholds similar enough to the molecular hydrogen data that the ratio is fairly constant.

For H_β emission, the variation in the ratio was more pronounced, changing rapidly from 1.18 at threshold to 1.11 at 100 eV. Again this is in disagreement with the data of Vroom and de Heer.[8] However, the 1.11 limit was reached at 30 eV, just above the threshold for dissociation through the $^1\Sigma_g^+(2p\sigma_u)^2$ state.

The ratio for H_γ varied from a factor of 2 near threshold to a value of 1.19 at 100 eV, in agreement with the data of Vroom and de Heer[8] at 100 eV. Again one notes that the ratio reached its high-energy limit when the electron energy exceeded the 35-eV threshold.

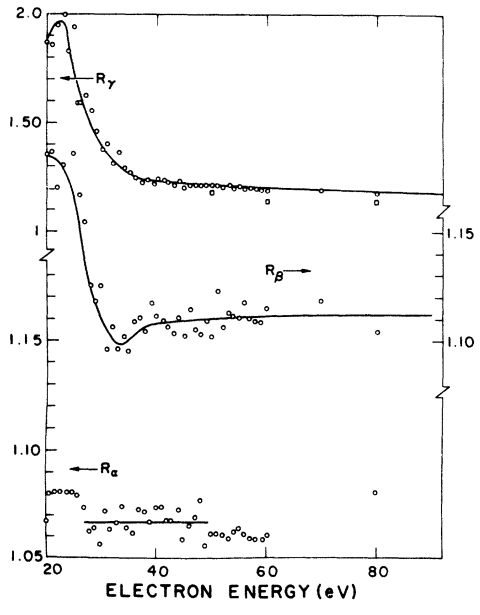

FIG. 9. Plot of the measured ratios R_α, R_β, and R_γ, the ratios for H_α, H_β, and H_γ emission cross sections for molecular hydrogen to respective cross sections for H_α, H_β, and H_γ emission from molecular deuterium. Note that the scales differ for the different ratios, and that the origins of coordinates are suppressed. The arrows indicate the scale used for each ratio.

From theoretical considerations, it is expected that an isotope effect should exist. Hazi[47] predicted that for dissociation through the $^1\Sigma_g^+(2p\sigma_u)^2$ state 40% of the H_2 atoms would decay to the dissociation continuum. For D_2 the corresponding number is 33%. The ratio of these probabilities is 1.2, in agreement with the present results above 30 eV.

At lower energies, of the two processes leading to dissociation, predissociation has relatively little isotopic dependence, while direct dissociation from the repulsive part of the $(1s\sigma_g)(nl)$ potential curve should show a large isotopic effect due to the Franck-Condon principle. Thus, since predissociation is more important for H_α production than for H_γ production, it is expected that dissociations producing H_α radiation will show less isotopic dependence than that producing H_γ radiation.

We follow the analysis of Bardsley *et al.*[53] and assume that the cross section is given by

$$Q_{\text{diss}} = Q_0 e^{-\Gamma\tau/\hbar}, \tag{11}$$

where Q_0 is the cross section for initial excitation to the $^1\Sigma_g^+(2p\sigma_u)^2$ state, $\hbar/\Gamma$ is the mean value of the lifetime of the state, and τ is the time it takes for the two atoms to separate such that no dissociation can occur after τ. For different isotopes τ will be proportional to the inverse square root of the reduced mass. For the present case,

$$R = Q_{\text{diss}}(H_2)/Q_{\text{diss}}(D_2) = \exp[(\Gamma\tau/\hbar)(\sqrt{2}-1)]; \tag{12}$$

for a ratio of 1.2, $\Gamma\tau \simeq 2.89\times10^{-16}$ eV sec. The separation time τ is typically 1×10^{-14} sec. Then $\Gamma \simeq 2.89\times10^{-2}$ eV. If one takes the region from zero separation to 2 Å, the mean values of Γ are much smaller than the width calculated by Bottcher and Docken[37,38] for the $^1\Sigma_g^+$ and $^3\Pi_g$ states but comparable to the width of the $^3\Sigma_u^+$ state. However, if the value of $\Gamma\tau$ is replaced in Eq. (12), one finds $Q_{\text{diss}} = 0.64Q_0$. This is in agreement with the ratio found by Hazi.[47] It is probable that the $^3\Sigma_u^+$ state behaves in a manner quite similar to the $^1\Sigma_g^+$ state and thus could be an important channel for production of excited atoms.

VIII. DEPENDENCE OF DISSOCIATION ON THE PRINCIPAL QUANTUM NUMBER

It is of interest to see if any power-law dependence exists for dissociation in a manner similar to that of electron transfer[54,55] and electron excitation[56] of atoms to states with large principal quantum numbers.

The true cross sections Q_n for excitation to state n are related to the measured emission

TABLE I. Measured power-law dependence x of the dissociation cross section at 100 eV. Each column with a heading $n/(n+y)$ tabulates the values of x derived from the data of the investigator (listed on the same horizontal line) using the pair of cross sections Q_n and Q_{n+y}. The last two horizontal lines give the average value of x and its standard deviation for that $n/(n+y)$ combination, the average including data of all investigators. The last column tabulates average values found using the data of each reference. The values used for the data of Ref. 58 may be inaccurate, the numbers used for cross sections were read off drawings.

	$n/(n+y)$						Average of
	$\frac{3}{4}$	$\frac{3}{5}$	$\frac{4}{5}$	$\frac{3}{6}$	$\frac{4}{6}$	$\frac{5}{6}$	each reference
Williams *et al.*[6]	5.287	5.225	5.127				5.21 ± 0.08
Vroom *et al.*[8]	4.63	4.906	5.242	4.616	4.608	3.822	4.64 ± 0.47
Present work	4.504	5.028	5.704				5.08 ± 0.60
Freund *et al.*[58]	4.15	4.480	4.891	4.434	4.64	4.325	4.49 ± 0.26
Average of $n/(n+y)$	4.64	4.90	5.24	4.53	4.62	4.07	
Standard deviation of $n/(n+y)$	0.47	0.31	0.34	0.13	0.02	0.36	

Average of all data: $x = 4.76 \pm 0.46$
Average of data excluding Ref. 58: $x = 4.99 \pm 0.37$

cross sections $\sigma_{n\to 2}$ through the branching ratios, such that

$$Q_n = \sigma_{n\to 2}/f_n , \tag{13}$$

where f_n is the fraction of the excited atoms in state n that radiate the Balmer line. These fractions depend on the orbital-state distribution

$$f_n = \sum_{l=0}^{n-1} Q_{nl} B_{l\to 2} \left(\sum_{l=0}^{n-1} Q_{nl} \right)^{-1} , \tag{14}$$

where $B_{l\to 2}$ is the branching ratio for radiation to the $n=2$ level from a given orbital state nl. Since no theoretical values were predicted for the ratios of the different cross sections Q_{nl}, four models were used: $Q_{ns} = Q_{np} = Q_{nd}$; $2Q_{ns} = Q_{np} = 2Q_{nd}$; $Q_{ns} = 0$, $Q_{np} = Q_{nd}$; and $Q_{ns} = 0$, $Q_{np} = 2Q_{nd}$. The values of f_n were found to be $f_3 = 0.56 \pm 0.12$, $f_4 = 0.42 \pm 0.08$, $f_5 = 0.40 \pm 0.06$, and $f_6 = 0.33 \pm 0.04$, where the uncertainty represents the spread in f among the four models.

Let us assume $Q_n = K/n^x$. Then by measuring Q_{n+y} and Q_n it is necessary that

$$x = \frac{\ln(Q_n/Q_{n+y})}{\ln[(n+y)/n]} = \frac{\ln(f_{n+y}\sigma_{n\to 2}/f_n\sigma_{n+y\to 2})}{\ln[(n+y)/n]} . \tag{15}$$

Thus by taking ratios of measured emission cross sections, x can be determined. Table I summarizes the values found using the different data at 100 eV; Table II summarizes the values found at 22 eV. It is immediately obvious that two different power laws exist, the one for direct dissociation being 6.5±1.0 and the one at higher energies being 5.0±0.5, where the uncertainties represent one standard deviation of the mean. If one includes the estimated uncertainties in f_n, then x would change by at most 20%, and probably a common power law of 5.5±1.25 would be consistent with the available data.

ACKNOWLEDGMENTS

The author would like to thank Dr. S. J. Smith for support and encouragement during the course of this work, Dr. G. H. Dunn for numerous discussions as well as for lending some of the in-

TABLE II. Same as Table I, but at 20 eV.

Reference	$n/(n+y)$						Average of
	$\frac{3}{4}$	$\frac{3}{5}$	$\frac{4}{5}$	$\frac{3}{6}$	$\frac{4}{6}$	$\frac{5}{6}$	each reference
Williams *et al.*[6]	5.96	7.28	6.20				6.48 ± 0.57
Present work	7.49	6.94	6.22				6.88 ± 0.64
Freund *et al.*[58]	5.74	5.87	6.02	5.56	5.45	4.74	5.56 ± 0.45
Average of $n/(n+y)$	6.39	6.70	6.15				
Standard deviation of $n/(n+y)$	0.95	0.74	0.09				

Average of all data: $x = 6.35 \pm 1.14$
Average of all data excluding Ref. 58: $x = 6.68 \pm 0.58$

terference filters used in the present work, Dr. P. O. Taylor for allowing the use of his calibrated radiation transfer source, and Dr. A. V. Phelps.

APPENDIX: LOSS OF HIGH VELOCITY ATOMS

In Sec. VI it was demonstrated that at electron energies greater than 30 eV the dissociation products move with velocities between 8 and 9 km/sec. Since the detection assembly samples a finite region of space, loss of some of these atoms from the observation region was unavoidable. The amount of radiation lost depend on the lifetime of the atoms being observed.

If one considers the observation region as a cylindrical section whose axis is parallel to the electron beam, then atoms lost to the outside of the observation region along the direction of the electron beam were compensated by atoms scattered into the observation region along the direction of the electron beam axis. This was true provided the electrons experienced single collisions and provided the target pressure was low enough for the mean free path of the excited atoms to be greater than the dimensions of the scattering region.

Thus attention should be focused on the radial direction, the worst case being that in which the velocity is radial. This is the case considered here. Let us assume that the electron beam density is uniformly distributed in a square cylinder whose sides are parallel to the three axes of the scattering geometry. The production density of radiators in a direction normal to the electron beam axis is given by

$$\rho(x)=\begin{cases}0, & w\leq x,\\ \rho_0, & -w\leq x\leq w,\\ 0, & x\leq -w,\end{cases} \tag{A1}$$

where $\rho_0(x)=N_0/2w$, w is the half-width of the beam, and N_0 is the total number of radiators in the collision volume. Note that x is perpendicular to the electron beam axis as well as to the optics axis. Since the probability of decay is exponential, the normalized probability density for decay a distance y from the point where the atom is excited is given by

$$P(y)=\frac{1}{2\sigma}\exp\left(-\frac{|y|}{\sigma}\right),\quad \int_{-\infty}^{\infty}P(y)\,dy=1, \tag{A2}$$

where σ is the decay length.

Thus the number density of radiators that decay at a distance d from the origin of coordinates (the electron beam axis) is given by

$$N(d)=\int_{-\infty}^{\infty}\rho(x)P(d-x)\,dx, \tag{A3}$$

which is equal to

$$N(d)=\begin{cases}(N_0/2w)e^{-|d|/\sigma}\sinh(w/\sigma), & |d|>|w|,\\ (N_0/2w)[1-e^{-w/\sigma}\cosh(y/\sigma)], & |d|<|w|.\end{cases} \tag{A4}$$

Thus the fraction of atoms that decay between $\pm\Delta$ is given by

$$F(\Delta)=\frac{\int_{-\Delta}^{\Delta}N(d)\,dd}{\int_{-\infty}^{\infty}N(d)\,dd}=\frac{2}{N_0}\int_{-\Delta}^{\Delta}N(d)\,dd. \tag{A5}$$

The value of $F(\Delta)$ goes to the correct limit 1 if σ is not infinite but Δ is infinite, and goes to zero if σ is infinite but Δ is finite. Similarly, if w is zero (a line source) then only $1/2\sigma$ of the radiation is detected, the exact fraction for a line source.

Substituting a value of 0.08 cm for the half-width of the electron beam and 0.15 cm for the half-width of the observation region, a value of F is calculated as a function of $\sigma=v\tau$, where v is the velocity of the atom and τ is the lifetime of the radiator. Figure 10 is a plot of the calculated fraction F. The values of the fraction for the different states of interest are also indicated. The subscript F refers to fast atoms (40 km/sec), while the label S refers to slow atoms (8 km/sec).

If one assumes a distribution of excited states, $Q_{np}=2Q_{nd}=4Q_{ns}$, $Q_{nl}=0$ otherwise, then for H_α less than 13% of the fast atoms were not observed, while for H_β less than 20% of the fast atoms were not observed, and less than 26% of

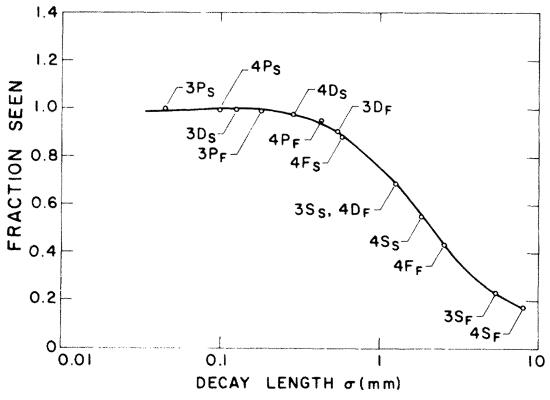

FIG. 10. Plot of the fraction of atoms that decay within an observation region of half-width 1.5 mm. The horizontal axis represents the decay length $\sigma=v\tau$. Indicated on the graph are the values for different atoms with different states nl_S or nl_F. n indicates the principal quantum number of the state, l is the orbital quantum number, S refers to slow atoms (8 km/sec), and F refers to values obtained for fast atoms (40 km/sec).

the fast H_γ-emitting atoms were not observed.

These are the worst cases. In actual practice the beam was not uniformly distributed, and its cross section was not square. The beam was cylindrical in cross section and its density was Gaussian in shape. The product of these two factors was seen in Fig. 3. Thus in practice these worst cases are off by more than a factor of 2. The effect of the loss was not included in the reduction of the data, since a much better understanding of the orbital distribution of the cross section is needed before such a procedure is valid. It is expected[10,57] that almost no states with orbital angular momentum quantum number $l = 0$ are produced. If that is the case, then the present worst-case model gives losses of 3%, 5%, and 10%, respectively, for H_α, H_β, and H_γ radiation at high energies of the incident electrons.

---

*Work supported by the National Science Foundation under Contract No. GP-39308X, through the University of Colorado.

[1]G. J. Schulz and R. K. Asundi, Phys. Rev. Lett. 15, 946 (1965).
[2]A. Crowe and J. W. McConkey, J. Phys. B 6, 2088 (1973), and references therein.
[3]M. Misakian and J. C. Zorn, Phys. Rev. A 6, 2180 (1972), and references therein.
[4]D. M. Cox and S. J. Smith, Phys. Rev. A 5, 2428 (1972).
[5]J. A. Schiavone, K. C. Smyth, and R. S. Freund, J. Chem. Phys. 63, 1043 (1975).
[6]E. R. Williams, J. V. Martinez, and G. H. Dunn, Bull. Am. Phys. Soc. 12, 233 (1967); G. H. Dunn, private communications.
[7]K. M. Burrows and G. H. Dunn, Bull. Am. Phys. Soc. 13, 215 (1968); G. H. Dunn, private communication.
[8]D. A. Vroom and F. J. de Heer, J. Chem. Phys. 50, 580 (1969).
[9]L. D. Weaver and R. H. Hughes, J. Chem. Phys. 52, 2299 (1970).
[10]L. Julien, M. Glass-Maujean, and J. P. Descoube, J. Phys. B 6, 1196 (1973).
[11]M. Glass-Maujean, in *Proceedings of the Fourth International Conference on Atomic Physics, Abstracts of Contributed Papers, Heidelberg, 1974,* edited by J. Kowalski and H. G. Weber (Heidelberg U. P., Heidelberg, 1974), p. 260.
[12]J. D. Walker, Jr., and R. M. St. John, J. Chem. Phys. 61, 2394 (1974).
[13]C. B. Richardson, B. P. Gilstrap, and R. H. Hughes, Bull. Am. Phys. Soc. 20, 466 (1975).
[14]A. H. Mahan, A. Gallagher, and S. J. Smith, Phys. Rev. A 13, 156 (1976).
[15]A. H. Mahan and A. Gallagher, Rev. Sci. Instrum. 47, 81 (1976).
[16]A. M. Mahan, R. V. Krotkov, A. C. Gallagher, and S. J. Smith, Bull. Am. Phys. Soc. 18, 1506 (1973).
[17]G. A. Khayrallah and S. J. Smith, in *Electronic and Atomic Collisions, Abstracts of the Papers of the Ninth International Conference on the Physics of Electronic and Atomic Collisions,* edited by J. S. Risley and R. Geballe (University of Washington Press, Seattle, 1975), p. 808.
[18]R. S. Freund, J. A. Schiavone, D. F. Brader, and K. C. Smyth, in Ref. 17, p. 810.
[19]R. L. Long, D. M. Cox, and S. J. Smith, J. Res. Natl. Bur. Stand. A 72, 521 (1968).
[20]E. A. Soa, Jenaer Jahrb. 1, 115 (1959).
[21]Veeco model RG-75, with a Veeco model RG-21A controller.
[22]Varian model 971-5009, with a Varian controller model 971-0014.
[23]D. M. Cox, Ph.D. thesis (University of Colorado, 1970) (unpublished).
[24]RCA model C31034 photomultiplier.
[25]L. R. Wilcox and W. E. Lamb, Jr., Phys. Rev. 199, 1915 (1960).
[26]D. W. O. Heddle, Proc. Phys. Soc. Lond. 90, 81 (1967).
[27]W. E. Lamb, Jr., and T. M. Sanders, Phys. Rev. 119, 1901 (1960).
[28]G. H. Dunn kindly lent this filter for use in this experiment.
[29]A. L. Hughes and P. Lowe, Phys. Rev. 21, 292 (1923); W. H. Crew and E. O. Hulbert, Phys. Rev. 29, 843 (1927); S. Vencov, Ann. Phys. (Paris) 15, 131 (1931).
[30]A. S. Coolidge, Phys. Rev. 65, 236 (1944).
[31]H. G. Gale, O. S. Monk, and K. O. Lee, Astrophys. J. 67, 89 (1928).
[32]H. M. Crosswhite, *The Hydrogen Molecule Wavelength Tables of Gerhard-Heinrich Dieke* (Wiley-Interscience, New York, 1972).
[33]P. O. Taylor, Ph.D. thesis (University of Colorado, 1972) (unpublished), and private communication.
[34]G. H. Dunn has very kindly provided his unpublished curves for inclusion in Figs. 5–7. The absolute values of these cross sections as published in Ref. 6 are being revised to an absolute accuracy of 3%.
[35]The preliminary results shown in Fig. 2 of Ref. 17 were drawn incorrectly for electron energies below 90 eV.
[36]G. H. Dieke, J. Mol. Spectrosc. 2, 494 (1958).
[37]C. Bottcher and K. Docken, J. Phys. B 7, L5 (1974).
[38]C. Bottcher, J. Phys. B 7, L352 (1974).
[39]A. U. Hazi, J. Phys. B 8, L262 (1975).
[40]T. E. Sharp, At. Data 2, 119 (1971).
[41]J. A. Schiavone, K. C. Smyth, and R. S. Freund, J. Chem. Phys. 63, 1043 (1975).
[42]W. E. Lamb, Jr., and R. C. Retherford, Phys. Rev. 79, 549 (1950).
[43]A. U. Hazi, Chem. Phys. Lett. 25, 259 (1974).
[44]G. H. Dunn, Phys. Rev. Lett. 8, 62 (1962).
[45]T. F. O'Malley, J. Chem. Phys. 51, 322 (1969).
[46]C. Bottcher, Proc. R. Soc. A 340, 301 (1974).
[47]A. U. Hazi, J. Chem. Phys. 60, 4358 (1974).
[48]R. A. Phaneuf, D. H. Crandell, and G. H. Dunn, Phys. Rev. A 11, 528 (1975).
[49]A. Crowe and J. W. McConkey, Phys. Rev. Lett. 31,

192 (1973); J. Phys. B 6, 2088 (1973). The results of these references may be incorrect because of the unknown transmission function of their apparatus.
[50]J. A. D. Stockdale, V. E. Anderson, A. E. Carter, and L. Deleanu, J. Chem. Phys. 63, 3886 (1975).
[51]A. L. Ford and K. K. Docken, J. Chem. Phys. 62, 4955 (1975).
[52]D. A. Vroom and F. J. de Heer, J. Chem. Phys. 50, 573 (1969).
[53]J. N. Bardsley, A. Herzenberg, and F. Mandl, Proc. Phys. Soc. Lond. 89, 321 (1966).
[54]G. A. Khayrallah, R. Karn, P. M. Koch, and J. E. Bayfield, in *Proceedings of the Seventh International Conference on the Physics of Electronic and Atomic Collisions, Amsterdam, 1971, Abstracts of Papers*, edited by L. M. Branscomb *et al.* (North-Holland, Amsterdam, 1971), pp. 813 and 814.
[55]J. E. Bayfield, G. A. Khayrallah, and P. M. Koch, Phys. Rev. A 9, 200 (1974).
[56]K. Omidvar, Phys. Rev. A 12, 913 (1975).
[57]V. A. Ankudinov, S. V. Bobashev, and E. P. Andreev, Zh. Eksp. Teor. Fiz. 52, 364 (1967) [Sov. Phys.—JETP 25, 236 (1967)].
[58]R. S. Freund, J. A. Schiavone, and D. F. Brader (to be published).

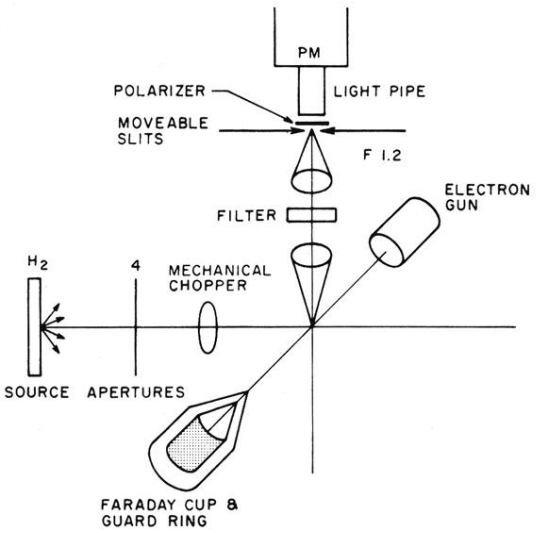

FIG. 1. Schematic diagram of the apparatus. The electron beam axis, the atomic beam axis, and the photomultiplier assembly axis are mutually orthogonal.